Critical Micelle Concentration of an Ammonium Salt Through DPD Simulations Using COSMO-RS–Based Interaction Parameters

Raúl Oviedo-Roa
Grupo de Química Aplicada a la Industria Petrolera, Programa de Ingeniería Molecular, Instituto Mexicano del Petróleo, Eje Central Lázaro Cárdenas Norte 152, Col. San Bartolo Atepehuacán, Gustavo A. Madero, México 07730, D.F., México

José M. Martínez-Magadán
Grupo de Química Aplicada a la Industria Petrolera, Programa de Recuperación de Hidrocarburos, Instituto Mexicano del Petróleo, Eje Central Lázaro Cárdenas Norte 152, Col. San Bartolo Atepehuacán, Gustavo A. Madero, México 07730, D.F., México

Ana Muñoz-Colunga
Grupo de Química Aplicada a la Industria Petrolera, Programa de Ingeniería Molecular, Instituto Mexicano del Petróleo, Eje Central Lázaro Cárdenas Norte 152, Col. San Bartolo Atepehuacán, Gustavo A. Madero, México 07730, D.F., México

Rodolfo Gómez-Balderas
Laboratorio de Fisicoquímica Analítica, Unidad de Investigación Multidisciplinaria, Facultad de Estudios Superiores Cuautitlán, Universidad Nacional Autónoma de México, Carr. Cuautitlán-Teoloyucan, Km. 2.5, San Sebastián Xhala, Cuautitlán Izcalli, Estado de México 54714, México

Mirna Pons-Jiménez
Grupo de Química Aplicada a la Industria Petrolera, Programa de Posgrado, Instituto Mexicano del Petróleo, Eje Central Lázaro Cárdenas Norte 152, Col. San Bartolo Atepehuacán, Gustavo A. Madero, México 07730, D.F., México

Luis S. Zamudio-Rivera
Grupo de Química Aplicada a la Industria Petrolera, Programa de Ingeniería Molecular, Instituto Mexicano del Petróleo, Eje Central Lázaro Cárdenas Norte 152, Col. San Bartolo Atepehuacán, Gustavo A. Madero, México 07730, D.F., México

DOI 10.1002/aic.14158
Published online July 1, 2013 in Wiley Online Library (wileyonlinelibrary.com)

In order to determine the critical micelle concentration (CMC) of aqueous dodecyltrimethylammonium chloride (DTAC), a screening of the DTAC gathering process at different molalities by performing dissipative particle dynamics (DPD) simulations over mesomolecules whose beads interact via repulsive conservative forces was performed. Conductor-like screening model for real solvent quantum methodology, applied to molecular segments that describe the DTAC chemistry and were mapped onto the DPD beads, allows us the computing of activity coefficients at infinite dilution to obtain thermodynamic Flory–Huggins interaction parameters, from which we calculated the maxima repulsive conservative forces, that is, the DPD interaction parameters. Results indicate that at room temperature the CMC is 0.0217 mol/kg, the aggregation number ranges from 46 to 54 molecules, and the aggregate radius varies from 19.58 to 22.02 Å; all values are in excellent agreement with literature reported experimental ones of 0.0213 mol/kg, 47 ± 5 molecules, and 20.1 Å. © 2013 American Institute of Chemical Engineers *AIChE J*, 59: 4413–4423, 2013

Keywords: critical micelle concentration, dissipative particle dynamics, conductor-like screening model for real solvents, Flory–Huggins interaction parameter, infinite-dilution activity coefficient

Introduction

One of the major challenges in the oil industry is the recovery factor enhancement for mature fields possessing naturally fractured carbonate formations. In order to maintain

Correspondence concerning this article should be addressed to R. Oviedo-Roa at oviedor@imp.mx.

the reservoir pressure and increase the recovery factor after primary recovery, waterflood processes have been implemented.[1,2] However, fractured carbonate reservoirs have the characteristic of possessing oil- or oil–water-mixed-wettability because of the adsorption of acidic components present in the crude oil,[3,4] consequently, the capillary driving force, for the spontaneous imbibition process of water, is weak and, therefore, the oil migration from matrix to fractures is poor or null, leading to low waterflooding oil recoveries.[5] It has been reported in a series of articles[6–14] that the recovery efficiency from naturally fractured carbonate reservoirs can be improved by dissolving in the injection water cationic surfactants of the type tetraalkylammonium salts, $R{-}N(CH_3)X$ ($R = C_n$, $8 \leq n \leq 16$, X = Cl or Br), thereby achieving to alter the wettability of the reservoir rock to become more water wet. The extensive experimental work concludes that cationic surfactants are able to irreversibly desorb carboxylic materials from the chalk surface via the formation of ion pairs between the surfactant cationic heads and the anion components of crude oil.

For those $R{-}N(CH_3)X$ at concentrations above the critical micelle concentration (CMC), two main facts occur: the imbibition rate and total recovery increase as the cationic surfactant concentration increases,[6] and the contact angle of water in air on the chalk surface decreases to zero.[14] For the values well above the CMC, the total recovery decreased with increasing surfactant concentration; it has been rationalized in terms of the solubilization, by means of micelles, of oil recovered in the surfactant solution. At concentrations below the CMC, the potential to expel oil from the rock decreases drastically.[6] All these suggest that there exists an optimum surfactant concentration for cationics, typically above the CMC, for a considerable wettability alteration that leads to an effective oil recovery by capillary imbibition in chalks.

Conversely, computational molecular modeling and computer simulation combine methods that cover a size range of spatial and time scales, going from the subatomic scale of the quantum mechanics, passing by the atomistic and nanoscale level of the molecular mechanics, molecular dynamics, and Monte Carlo methods, among others, up until the micrometric focus of the mesoscale modeling.[15] The quantum mechanics methods allow the simulation of systems containing hundreds of atoms. The molecular mechanics is an appropriate method to calculate the structure and behavior of larger molecular systems. The mesoscale modeling can study even larger molecular systems and is particularly useful in the study of the hydrodynamic behavior of polymers and soft materials, and of the nanocomposite morphology[16,17]; it uses a basic unit, an agglomeration of atoms called bead, obtained through a coarse-graining mapping procedure. An example of mesoscale theories is the dissipative particle dynamics (DPD).[18]

DPD have been used to simulate ammonium quaternary salts such as cetyltrimethylammonium bromide (CTAB) at oil/water interface. Three different microstructures, spherical oil in water, interfacial phase, and water in oil, were observed with the oil/water ratio increasing; besides, it was shown that CTAB has a high interfacial efficiency at the oil/water interface, that is, the increase of surfactant molar fraction from 0.004 to 0.1 corresponds to a 90% reduction of the interfacial tension.[19] By the analysis of the DPD simulated interface tension and microstructure, a phase diagram has been predicted, which is consistent with experimental results.[20] DPD simulations of the aggregation of CTAB in water and ethanol/water mixtures reflected that tail groups of CTAB interact more strongly with ethanol than with water, which elucidates the difficulty of micelles to form in ethanol.[21] A mesoscopic simulation study through the DPD method on the interaction between the hydrolyzed polyacrylamide polymer and C_{12}NBr (dodecyl-oxypropyl-β-hydroxyl trimethyl-ammonium bromide) or C_9phNBr (nonyl-phenyl-oxypropyl-β-hydroxyl trimethyl-ammonium bromide) in aqueous solution showed that C_{12}NBr is most likely to form polymer/surfactant complex in contrast to C_9phNBr, and the DPD results were validated via experiments of binding isotherms.[22] DPD simulations can be used to predict interfacial tensions and its modification due to the presence of a surfactant in the interface between oil and water, and also to investigate the wettability alteration of dolomite reservoir rock surfaces by surfactant aqueous solutions,[23] as well as the increase of the contact angle of an oil drop on a dolomite rock surface in a surfactant aqueous solution medium, relative to that obtained in pure water, due to a lowering of the interfacial tension at the water–oil interface, instead of rock–fluid interfacial tension.[24]

Originally, the mesoscopic simulation technique DPD is aimed to simulate soft spherical beads interacting through a pair-wise potential, and thermally equilibrated through hydrodynamics evolution.[25,26] Then, the methodology was extended to describe polymeric and surfactant systems by introducing bead-and-spring type models.[27–29] A bead represents several atoms of a molecular fragment owning a specific chemistry that are lumped together into a single simulation particle.[30] The total force on each DPD particle is expressed as a sum of three pair-wise additive terms: (1) a conservative force, which is taken to be a soft repulsion; (2) a dissipative force, proportional to the relative velocity of the beads; and (3) a random force, necessary to maintain the system temperature.[31] For molecules of various monomers an additional force, coming from the spring potential energy, must be included. Although the dissipative and random forces act in unison as a thermostat for the simulation evolution, it is the conservative soft repulsive force that embodies the essential chemical behavior of the system. This conservative pair-wise repulsive force f_{ij} between the beads i and j is characterized by a maximum value, a_{ij}, and it acts within a cutoff distance, r_{cutoff} [18]: $f_{ij}(r) = a_{ij}(1 - r/r_{\text{cutoff}})$ if $r \leq r_{\text{cutoff}}$; otherwise $f_{ij}(r) = 0$. The so-called DPD interaction parameter a_{ij} is related with the Flory–Huggins thermodynamic interaction parameter χ_{ij},[32] for a mixture of the molecular fragments represented by the beads i and j, through[18]

$$a_{ij} = 25 + 3.5\chi_{ij} \tag{1}$$

This a_{ij}–χ_{ij} relation, which holds when there are $\rho = 3$ beads within a r_{cutoff}^3 cubic volume, opened the way to do large scale simulations, realistically describing millions of atoms, by first performing simulations of molecular fragments retaining atomistic details to derive χ_{ij} parameters, then second using these results as input to a DPD simulation to study the formation of micelles, networks, mesophases, and so forth. There are several approaches suggested in polymer science, which link the χ_{ij} parameter to solubilities and mixing energies of the polymeric components.[33] For instance, the Monte Carlo method evaluates the averaged mixing energies $\langle E_{ij}^{\text{mix}} \rangle$ of two species from their pair contact energies,

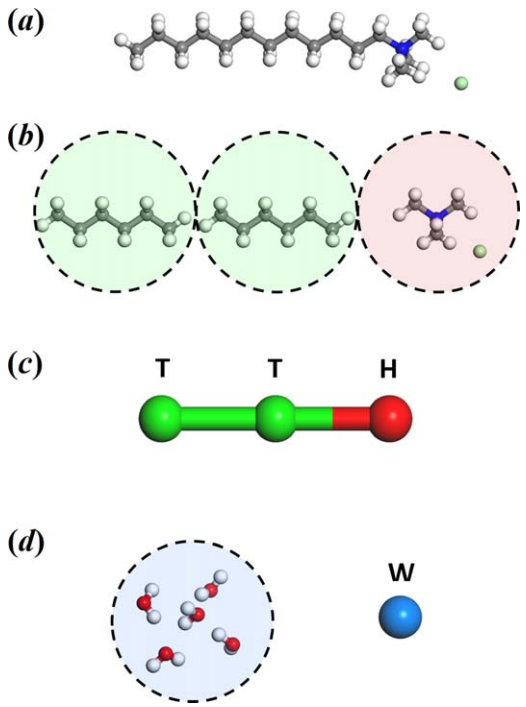

Figure 1. (a) Atomistic model for the DTAC molecule.

(b) Partition of DTAC into molecular segments. (c) Mesomolecular representation of a DTAC molecule. (d) Left: cluster of m water molecules contained within the volume of a bead. Right: Mesomolecule representing this cluster. (Atom colors: white, hydrogen; gray, carbon; blue, nitrogen; red, oxygen; green, chlorum. Bead colors: green, T; red, H; blue, W). [Color figure can be viewed in the online issue, which is available at wileyonlinelibrary.com.]

and then Flory–Huggins parameter is obtained as $\chi_{ij}=\langle E_{ij}^{\mathrm{mix}}\rangle/RT$.[34] Another extensively used method involves the δ_i solubility parameter, obtained from atomistic molecular dynamics simulations for pure species i, allowing the calculation of Flory–Huggins parameter as $\chi_{ij}=V_{\mathrm{b}}\left(\delta_i-\delta_j\right)^2/kT$,[35,36] where V_{b} is the DPD-bead volume. In a third approach, interaction repulsive DPD parameters a_{ij} are coupled to binding energy values between different species resulting from atomistic molecular dynamics simulations.[37] It is worthy to mention that in all these approaches, the interatomic interactions are described by forcefields,[38–40] that is, the connection from nanoscale to mesoscale is taken into account via classical simulations.

In this article, a procedure for transferring molecular information from quantum-atomistic scale to mesoscale is presented, and then applied to obtain the CMC of dodecyltrimethylammonium chloride (DTAC, Figure 1a) in aqueous solution, by means of computer DPD simulations of the micellization process for a series of ammonium quaternary salt concentrations at room temperature.

Methodology

Now, in this section, we provide the methodology used to generate input information involved in micelle formation DPD simulations for surfactant solution models, that is, we describe the coarse-grained process in which DTAC and water molecules are mapped into beads, then the quantum computational methodology used to calculate the DPD interaction parameters a_{ij}, and, finally, the relationship between real and simulation surfactant concentrations for mesoscopic runs.

Along this methodology, four different model entities will be considered: (1) the whole DTAC and water molecules that constitute the real system; (2) the substances to be actually mapped, that is, both the molecular fragments, which properly capture the chemical nature of segments of the DTAC molecule, and the water molecule itself; (3) beads representing the substances; and (4) mesomolecular models for the DPD simulations constituted by the beads.

From atomistic to mesoscale description of molecules

In the coarse-grained process to build up the DPD beads, it is a fundamental assumption that all bead types are of the same volume V_{b} even when representing distinct species.[36] In this manner, we have dissected the molecular structure of DTAC into three segments properly in view of their chemical nature (Figure 1b): a polar head composed of both the cation $[N(CH_3)_4]^{1+}$ along with the anion Cl^{1-}, forming a substance represented by the bead H, and the hydrophobic tail composed of two molecules of *n*-hexane, each one represented by a bead T. Consequently, the DTAC molecule is represented at the mesoscale through a so-called mesomolecule assembled with two beads T and one H (Figure 1c). For this article, we define the bead volume V_{b} as the ratio between the volume V_2 of the whole DTAC molecule (Figure 1a) and the number of beads of its mesomolecular representation, $\ell=3$

$$V_{\mathrm{b}}\equiv\frac{V_2}{\ell} \tag{2}$$

Particularly, in turn, water substance is represented through a bead W, whose volume V_{b} is filled by a cluster of m water molecules (Figure 1d), being m defined as

$$m\equiv\frac{V_{\mathrm{b}}}{V_1} \tag{3}$$

where V_1 is the volume of a single water molecule. The volumes V_1 and V_2 could be obtained at least by either of the following three different methods: (1) using experimental mass densities and molecular weights;* (2) performing forcefield-based molecular dynamics simulations at constant pressure and constant temperature;† and (3) combining a quantum chemical description of a molecule with an approximate continuum description of the surrounding solvent, such as in the conductor-like screening model (COSMO), further described. For methodological consistency with the quantum-atomistic–based calculations of the Flory–Huggins parameter χ_{ij} here proposed, we use the latter method. There, a solute molecular cavity is built up in the continuum solvent using atomic radii, typically in the range of 1.2 times Bondi radii.[41,42]

Statistical-thermodynamics-based relation to calculate Flory–Huggins interaction parameters

In order to compute the DPD interaction parameters a_{ij} between any pair of the above mentioned beads H, T, or W,

*The molecular volume can be estimated by means of $v=M/(N_A\cdot\rho)$, where M, N_A, and ρ are the molecular weight, Avogadro number, and mass density, respectively. This equation, however, provides actually the effective volume per molecule.

†The effective volume per molecule for one species is calculated through $v=V/N$, where V and N are the simulation cell volume and the total number of molecules contained in the cell, respectively.

it is necessary, owing to Eq. 1, to obtain the χ_{ij} Flory–Huggins interaction parameters for each one of the three possible binary condensed-phase molecular mixtures, specifically: $[N(CH_3)_4]Cl$/*n*-hexane, $[N(CH_3)_4]Cl/H_2O$, and *n*-hexane/H_2O pairs. According to the liquid lattice theory, χ_{ij} is determined from the original μ_{ij}-χ_{ij} Flory–Huggins thermodynamics relation (Eq. 4, below). In Eq. 4, μ_{ij} is the chemical potential of the solvent i in mixing with the solute j. Explicitly, for binary solutions in which the solute has higher molecular volume than solvent

$$\mu_{ij}(\phi_j)-\mu_i^{\mathrm{P}}(0)=RT\left[\ln\left(1-\phi_j\right)+\left(1-\frac{1}{r_{ij}}\right)\phi_j+\chi_{ij}\phi_j^2\right] \quad (4)$$

where μ_i^{P} is the standard state chemical potential of the pure solvent, $r_{ij}=v_j/v_i$ is the ratio of molecular volume of the solute to that of the solvent, and ϕ_j is the volume fraction of the solute in the binary solution.

Conversely, left-side term of Eq. 4 can be related to the solvent activity coefficient γ_{ij} by the equation[43]

$$\ln\left(x_i\gamma_{ij}\right)=\frac{\mu_{ij}-\mu_i^{\mathrm{P}}}{RT} \quad (5)$$

being x_i the mole fraction of solvent i. The liquid lattice theory replaces the mole fractions by volume fractions; therefore, in terms of the ϕ_j solute volume fraction, x_i is expressed as[‡]

$$x_i=\frac{1-\phi_j}{1-\left(1-\frac{1}{r_{ij}}\right)\phi_j} \quad (6)$$

Now, combining Eqs. 4–6, the χ_{ij} Flory–Huggins interaction parameter can be calculated from the expression[44,45]

$$\chi_{ij}=\frac{\ln\left(\gamma_{ij}\right)-\ln\left[1-\left(1-\frac{1}{r_{ij}}\right)\phi_j\right]-\left(1-\frac{1}{r_{ij}}\right)\phi_j}{\phi_j^2} \quad (7)$$

In the Flory–Huggins liquid lattice theory, the mixing enthalpy $\Delta H_{\mathrm{mix,ij}}$ is connected with χ_{ij} through $\Delta H_{\mathrm{mix,ij}}=kT\chi_{ij}\cdot v_i\phi_j$, where v_i is the number of solvent molecules i.[32] The product $v_i\phi_j$ is the average number of neighbor contacts among unlike molecules; thus, the maximum transferred mixing heat around sites of molecules i would occur when these sites are coordinated exclusively by sites of molecules j, namely, when $\phi_j\rightarrow 1$. As a result, the a_{ij} DPD maximum repulsion forces must be calculated through the infinite dilution limit of χ_{ij}[45]

$$\chi_{ij}^{\infty}\equiv\lim_{\phi_j\rightarrow 1}\chi_{ij}=\ln\left(\gamma_{ij}^{\infty}\right)+\ln\left(r_{ij}\right)-\left(1-\frac{1}{r_{ij}}\right) \quad (8)$$

where γ_{ij}^{∞} is the infinite dilution activity coefficient of the solvent i in mixing with the solute j.

COSMO-RS calculation of the infinite dilution activity coefficients

We have used the conductor-like screening model for real solvents (COSMO-RS) quantum chemical theory[41,46] to *a priori* compute the natural logarithm of the infinite dilution activity coefficient, $\ln\left(\gamma_{ij}^{\infty}\right)$, requested in Eq. 8, by means of a statistical thermodynamics treatment of interacting surface charges of the molecules i and j. First, using the TURBOMOLE software[47] through TMoleX interface, Version 3.1 (2011), a density functional theory (DFT) based geometry optimization of each molecule is performed under the COSMO continuum solvation model,[48] that is, as if embedded in a dielectric medium via a molecular surface or cavity that is constructed around the molecule. Each segment of this surface is characterized by a screening charge density (SCD), which takes into account the electrostatic screening of the molecule by its surrounding and the back-polarization of the molecule. In general terms, the cavity surface is discretized in small segments. On each segment s, a constant SCD σ_s is assumed, which yields a screening charge $q_s=\mathcal{A}_s\sigma_s$, with $\mathcal{A}_s$ being the area of the segment. This allows the calculation of the Coulomb interaction matrix $\mathbf{A}$ of the segments. For the molecular charge distribution, that is, nuclear charges and electronic density, a new set of screening charges $q^*=\{q_s^*\}$ are calculated from the conductor condition of vanishing total potential: $\mathcal{V}^{\mathrm{total}}=\mathcal{V}^{\mathrm{molecule}}+\mathbf{A}q^*=0$; here, $\mathcal{V}^{\mathrm{molecule}}$ is the electrostatic potential produced by the molecule on the segments. Furthermore, the screening charges q_i of the dielectric medium (of permeability ε) are scaled from the screening conductor charges through $q_s=(\varepsilon-1)/\left(\varepsilon+\frac{1}{2}\right)q_s^*$. These screening charges are substituted again as an external field into the quantum formalism. At the end of the quantum chemical self-consistency and geometry optimization loops, the SCD supplied by the continuum on each position of the molecular contact surface is known.

Afterward, by using the COSMOthermX software,[49] a liquid mixture is considered under the COSMO-RS model, that is, as an ensemble of closely packed ideally screened molecules i and j in which an electrostatic interaction arises from the contact of the different SCDs calculated by TURBOMOLE. The link between the microscopic surface interaction energies and thermodynamic properties, such as the macroscopic activity coefficient γ_{ij} of the compound i in mixing with compound j, is provided by statistical thermodynamics calculation of the pseudochemical potential, $\mu_{ij}^{\mathrm{pseudo}}$, which is the standard or reference chemical potential μ_{ij} minus $RT\ln\left(x_i\right)$.[46,50] So, when the calculation of the activity coefficient is toggled in COSMOthermX run, the output gives the result of $\ln\left(\gamma_{ij}\right)=\left(\mu_{ij}^{\mathrm{pseudo}}-\mu_i^{\mathrm{P}}\right)/RT$,[41] which is equivalent to Eq. 5.[§]

The quantum chemical DFT TURBOMOLE runs used the resolution-of-the-identity approximation with a triple-zeta valence polarized atomic basis (def-TZVP)[51] and Becke-Perdew (BP, i.e., B88-VWN-P86) functional, where VWN stands for Vosko, Wilk, and Nusair.[52] For the purpose of COSMO-RS applications, COSMO calculations considered the molecules i and j as if each molecule was immersed in a perfect conductor ($\varepsilon=\infty$).[53] For both self-consistent-field and geometry optimization convergence cycles, energy difference threshold was set to 10^{-9} Ha. Corresponding to the method and basis set level of TURBOMOLE runs, COSMOthermX used the parameter file BP_TZVP_C21_0111.ctd,[50] which contains the parameters required to produce reliable, high quality calculations of physicochemical data. Then, the natural logarithm of the coefficient of activity at room temperature was evaluated at infinite dilution ($x_i=0$ and $x_j=1$); it is

[‡]*Equation 6 can be deduced by using the relations $x_j/x_i=n_j/n_i$, $\phi_j/\phi_i=n_jv_j/n_iv_i$, $x_i+x_j=1$, and $\phi_i+\phi_j=1$, where n_l ($l=i,j$) is the mole number of substance l in a binary mixture.*

[§]*Equation 5 is obtained by substituting $\mu_{ij}^{pseudo}\equiv\mu_{ij}-RT\ln\left(x_i\right)$ into $\ln\left(\gamma_{ij}\right)=\left(\mu_{ij}^{pseudo}-\mu_i^{P}\right)/RT$.*

Table 1. Molecular Volumes of Aqueous Solution Compounds and those of Species Represented by Beads

	Volume	
Molecule	Atomic Units	Å^3
H_2O	172.84	25.61
DTAC	2,684.16	397.75
$[N(CH_3)_4]Cl$	1,076.33	159.50
n-Hexane	980.59	145.31
Bead	V_b=132.58 Å^3	

For volume conversion, 1 atomic unit = 0.14819 Å^3.

worth to note that the pure "solvent" in COSMOthermX is actually the solute *j*.

For methodological consistency, as it has been mentioned, and because of cavity volumes in COSMO agree quite well with the molecular volumes derived from experimental density,[41] the COSMO molecular volumes reported in the output of the TURBOMOLE runs are taken for the evaluation of the ratios r_{ij} of molecular volume of the solute to that of the solvent. Once the values of $\ln\left(\gamma_{ij}^{\infty}\right)$ and r_{ij} are obtained, the DPD interaction parameters a_{ij} are calculated by combining Eqs. 1 and 8. Likewise, the volumes V_1 and V_2 (required at Eqs. 3 and 2, respectively) will be the COSMO molecular volumes of a single water molecule and a whole DTAC one, respectively.

Definition of the solvent–solute DPD system

We have performed mesoscopic simulations through DPD module of Materials Studio (MS), Version 6.0.0, by Accelrys. In aim of generating an input model of the solution system, we have converted surfactant concentrations *c* into φ_1^{DPD} and φ_2^{DPD} volumetric fractions of a DPD-simulation-cell filled by solvent water and solute DTAC mesomolecules, respectively, and set up the size of the DPD simulation cell.

From Figure 1, it can be realized that there will be N_1 water molecules per $N_1^{DPD}(=N_1/m)$ water mesomolecules, and N_2 DTAC molecules per $N_2^{DPD}(=N_2)$ DTAC mesomolecules. In this way, the numbers $N_{b,1}=N_1^{DPD}$ and $N_{b,2}=\ell N_2^{DPD}$ of beads belonging to water and DTAC mesomolecules in the DPD simulation cell, respectively, are

$$N_{b,1}=\frac{N_1}{m} \qquad N_{b,2}=\ell N_2 \tag{9}$$

The volume fractions are defined as $\varphi_s^{DPD}\equiv V_s^{cell}/V^{cell}$ $(s=1,\ 2)$, where $V^{cell}=N_bV_b$ and $V_s^{cell}=N_{b,s}V_b$ are the full volume of the DPD simulation cell and the partial volume occupied by mesomolecules *s*, respectively, with $N_b=N_{b,1}+N_{b,2}$ as the total number of beads contained in the DPD simulation cell, that is, φ_s^{DPD} equals the relative amount of beads belonging to mesomolecule *s*, $N_{b,s}/N_b$. As a consequence, $\varphi_2^{DPD}=1-\varphi_1^{DPD}$ and

$$\varphi_1^{DPD}=\frac{\frac{n_1}{m}}{\frac{n_1}{m}+\ell n_2} \tag{10}$$

where $n_s=N_s/N$ is the mole fraction of molecule *s* in the laboratory solution, and $N=N_1+N_2$ is the total number of all molecules in the solution (therefore, $n_2=1-n_1$). The solvent

Table 2. Molecular Volume Ratios r_{ij}, Natural Logarithm of Infinite Dilution Activity Coefficients γ_{ij}^{∞}, Flory–Huggins Interaction Parameters χ_{ij}^{∞} and DPD Interaction Parameters a_{ij}

Bead *i* (Solvent)	Bead *j* (Solute)	r_{ij}	$\ln\left(\gamma_{ij}^{\infty}\right)$	χ_{ij}^{∞}	a_{ij}
W	H	6.227	−2.2579	−1.2681	20.66
W	T	5.673	7.2214	8.1334	52.85
H	T	0.911	14.2369	12.9746	69.43

mole fraction n_1 connects with the solute DTAC molality *c* (mole number of solute per kg of solvent) as[¶]

$$n_1=\frac{1}{1+cM_1} \tag{11}$$

where M_1 is the molecular weight of the solvent water.

Conversely, the DPD simulation cell is a supercell composed of r_{cutoff}-side cubic unit cells allocating ρ beads each one. The extents of the DPD simulation cell are $L_x\times L_y\times L_z$, where L_k represents the number of unit cells in the direction k $(k=x,\ y,\ z)$; that is, the DPD space will be adimensional. Then, the total number of beads N_b contained within the simulation cell is

$$N_b=\ \rho\left(L_x\times L_y\times L_z\right) \tag{12}$$

and, finally, the number of water mesomolecules, N_1^{DPD}, and those of DTAC, N_2^{DPD}, are

$$N_1^{DPD}=\varphi_1^{DPD}N_b$$
$$N_2^{DPD}=\frac{\varphi_2^{DPD}N_b}{\ell} \tag{13}$$

Consequently, a precise computation of the corresponding number of real atoms that constitute the mapped DPD system can be done as $N_{atoms}=mZ_1N_1^{DPD}+Z_2N_2^{DPD}$, where $Z_1=3$ and $Z_2=51$ are the number of atoms of a molecule of water and DTAC, respectively (Figure 1).

Results and Discussion

The molecular COSMO volumes for DTAC and H_2O reported in Table 1 give the DPD bead volume of $V_b=132.58$ Å^3, which matches to the volume of $m=5.177$ water molecules. For calculations of the solute-to-solvent molecular volume ratios r_{ij} among substances represented by beads as reported in Table 2, water is taken as the default solvent in $[N(CH_3)_4]Cl/H_2O$ and *n*-hexane/H_2O mixtures, whereas in the $[N(CH_3)_4]Cl$/*n*-hexane mixture, former compound is taken as the solvent due to its electric dipolar moment. Values of the DPD interaction parameters a_{ij} among beads *i* and *j*, as calculated through γ_{ij}^{∞} and χ_{ij}^{∞} for solvent *i* in mixing with solute *j*, are also shown in Table 2. All diagonal a_{ii} DPD interaction parameters, not shown in Table 2, were assigned the value 25, according to Eq. 1, as the interaction parameters χ_{ii} are zero for the pure-substance in the Flory–Huggins theory.[**]

It is worthy to note that the Flory–Huggins interaction parameter χ_{WH}^{∞} for water at infinite dilution in the quaternary

[¶]*The molality is* $c=(N_2/N_A)/m_1^{tot}$, *where* $m_1^{tot}=N_1(M_1/N_A)$ *is the total mass of the* N_1 *molecules of solvent. Solving these equations along with* $N_2=N-N_1$, *one finds Eq. 11.*

[**]*The Flory–Huggins interaction parameter is defined as* $\chi_{ij}\equiv z\Delta\varepsilon_{ij}/kT$,[32] *where z is the lattice coordination number and* $\Delta\varepsilon_{ij}\equiv\varepsilon_{ij}-\left(\varepsilon_{ii}+\varepsilon_{jj}\right)/2$ *is the interchange energy per new formed contact, and* ε_{ij} *are the contact energies. Thus, as* $\Delta\varepsilon_{ii}=0$, *so* $\chi_{ii}=0$.

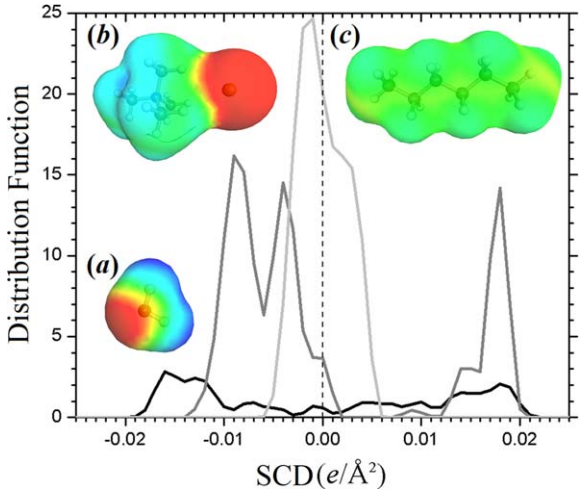

Figure 2. SCDs and their distribution functions for (a) water (black line), (b) $[N(CH_3)_4]Cl$ (gray line), and (c) *n*-hexane (light gray line).

Rainbow colors stand for: blue, negative SCDs; green, neutral SCDs; and red, positive SCDs. [Color figure can be viewed in the online issue, which is available at wileyonlinelibrary.com.]

nitrogen compound $[N(CH_3)_4]Cl$ is negative, that is, $a_{WH} < 25$, in agreement with Ref. 21 but contrasting with those $a_{WH} > 25$ obtained in Refs. 20 and 22 (these literature values were calculated from Monte Carlo simulations). Comparison in Figure 2 of the SCD profiles among water and $[N(CH_3)_4]Cl$ helps inferring the correct sign of χ^{∞}_{WH}.

The broad peaks around -0.015 and $+0.015$ $e/Å^2$ in the SCD profile of water (Figure 2a) reflect the ability of water to act as a charge acceptor as well as an donor, respectively; negative partial charges of atoms cause positive SCD and vice versa. When a charge acceptor in another compound has an SCD that is greater than $+0.01$ $e/Å^2$, or if a charge donor has an SCD that is below -0.01 $e/Å^2$, it can form hydrogen bonds with water.[46] The broad peak around $+0.015$ $e/Å^2$ in the $[N(CH_3)_4]Cl$ SCD-profile (Figure 2b), resulting from the chlorine atom, complements with the charge acceptor peak of water (-0.015 $e/Å^2$), whereas the peak at -0.010 $e/Å^2$ derived from the $[N(CH_3)_4]$ atoms, lies just at the edge to complement with the charge acceptor one ($+0.015$ $e/Å^2$). This means that water and $[N(CH_3)_4]Cl$ should mix quite favorably, that is, the corresponding change in the free energy of mixing, ΔG_{WH}, must be negative. In the Flory–Huggins theory,[32] $\Delta G_{ij} = RT\left(n_i \ln \phi_i + n_j \ln \phi_j + \chi_{ij} n_i \phi_j\right)$; thus, as $\phi_l \leq 1$, the entropic contributions satisfy $n_l \ln \phi_l \leq 0$ and, therefore, the limit at infinite dilution of water in $[N(CH_3)_4]Cl$ must lead to a negative χ^{∞}_{WH}. DPD runs performed for a mix of W and H bead monomers confirm that there is a homogeneous mixing (Figure 3a).

The *n*-hexane is the least polar fragment (Figure 2c). This is reflected in the narrow distribution of the charge densities for *n*-hexane in the SCD region around zero,[46] where the SCD of both water and $[N(CH_3)_4]Cl$ are relatively low; that is, there is an insufficient electrostatic interaction among *n*-hexane and these polar molecules, leading to phase separations among monomers of T bead and either W or H beads (Figures 3b,c), and, therefore, to positive values of both χ^{∞}_{WT} and χ^{∞}_{HT}.

Importantly, we can confirm the correct value of χ^{∞}_{WT}, and hence of a_{WT}, from experimental interfacial tension at 25°C among water and *n*-hexane, $\sigma = 51.10$ dyne/cm.[54] From the DPD run output for the mix among W and T bead monomers, it is obtained a dimensionless interfacial tension of $\sigma_{DPD} = 2.28$, which allows the calculation of the physical one through $\sigma = \left(kT/r^2_{cutoff}\right)\sigma_{DPD}$,[36] where

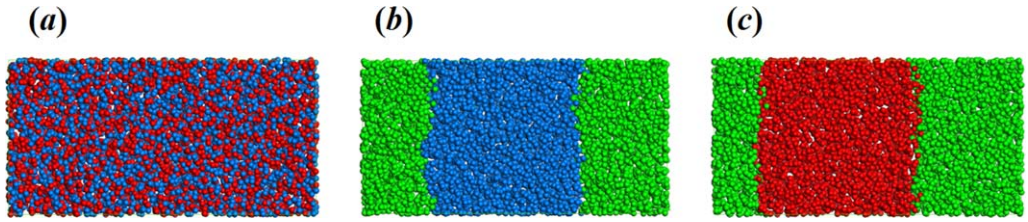

Figure 3. DPD simulations of 1:1 mixes among monomers of (a) W and H beads, (b) W and T beads, and (c) H and T beads.

Runs were performed in a 20×10×10 box with an equilibration period of 10,000 steps followed by a production stage of 50,000 steps. Bead colors as in Figure 1. [Color figure can be viewed in the online issue, which is available at wileyonlinelibrary.com.]

Table 3. Mole Fractions n_s, Volume Fractions φ_s^{DPD}, Number of Mesomolecules N_s^{DPD} (s=1, 2, or Equivalently, s= H_2O, DTAC), and Total Number of Real Atoms N_{atoms} Simulated in the Mixing Among Water and DTAC, all as Functions of the Concentration c of DTAC in Aqueous Solution

c (mol/kg)	n_{H_2O}	n_{DTAC}	$\varphi^{DPD}_{H_2O}$	φ^{DPD}_{DTAC}	$N^{DPD}_{H_2O}$	N^{DPD}_{DTAC}	N_{atoms}
c_1 = 0.0050	0.99991	0.00009	0.99860	0.00140	80,887	38	1,258,197
c_2 = 0.0100	0.99982	0.00018	0.99720	0.00280	80,773	76	1,258,365
c_3 = 0.0151	0.99973	0.00027	0.99580	0.00420	80,660	113	1,258,497
c_4 = 0.0201	0.99964	0.00036	0.99441	0.00559	80,547	151	1,258,680
c_5 = 0.0252	0.99955	0.00045	0.99301	0.00699	80,434	189	1,258,863
c_6 = 0.0302	0.99946	0.00054	0.99161	0.00839	80,320	227	1,259,030
c_7 = 0.0353	0.99936	0.00064	0.99021	0.00979	80,207	264	1,259,162
c_8 = 0.0404	0.99927	0.00073	0.98882	0.01118	80,094	302	1,259,345
c_9 = 0.0455	0.99918	0.00082	0.98742	0.01258	79,981	340	1,259,528
c_{10} = 0.0507	0.99909	0.00091	0.98602	0.01398	79,868	377	1,259,660

For calculations of n_s, we have used the water molecular weight value of 0.018015 kg/mol.

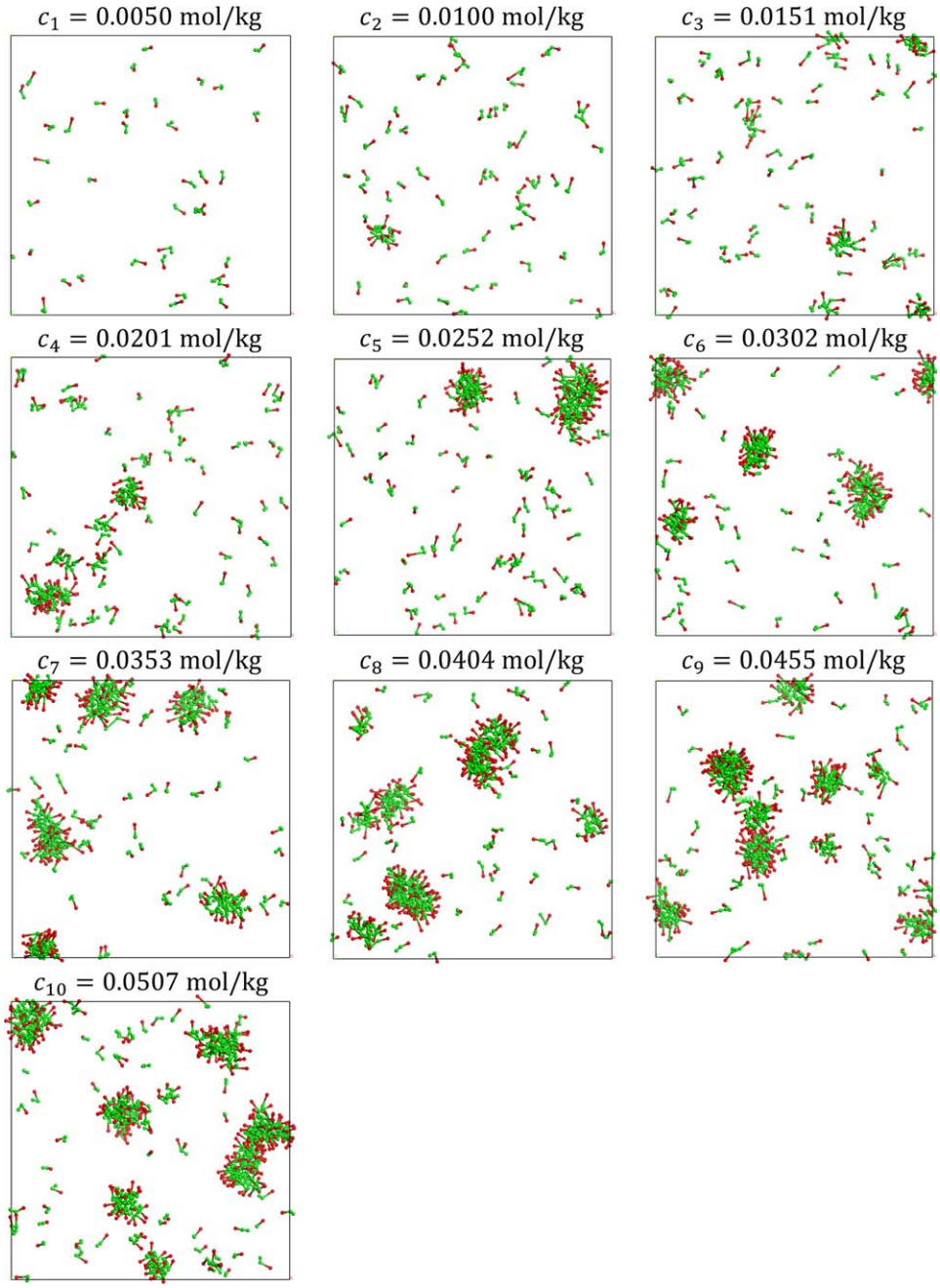

Figure 4. Images of DTAC distribution at the end of 100,000 steps of DPD simulations and for the selected molalities.

[Color figure can be viewed in the online issue, which is available at wileyonlinelibrary.com.]

$$r_{\text{cutoff}} = \sqrt[3]{\rho V_b} \tag{14}$$

In general, the Flory–Huggins interaction parameter χ_{ij} characterizes the interaction energy per solvent monomer divided by kT[32]; in particular, χ^{∞}_{WT} measures the interacting energy within a volume equal to that of a water molecule. Thus, for the binary W-T bead monomer mix (Figure 3b) we set $V_b^{WT} = V_1$, which gives $r_{cutoff}^{WT} = 4.25$ Å and, consequently, $\sigma = 51.93$ dyne/cm, in excellent agreement with the above experimental value as it deviates only 1.6%, validating our DPD interacting parameter a_{WT}. Beside, as peaks of the $[N(CH_3)_4]Cl$ SCD-profile are more intensive than those of water, it is expected a stronger repulsion among $[N(CH_3)_4]Cl$ and *n*-hexane than that among water and *n*-hexane. Thus, the fact that the H/T interface is most flat than the W/T one (Figures 3b,c) is due to $a_{HT} = 69.43 > a_{WT} = 52.85$ (Table 2).

We have set the DPD-simulation-cell dimensions at 30×30×30 unit cells; thus, it contains 81,000 beads, which are representing around 1.26 millions of atoms. Table 3 shows in gray columns the volume fractions φ^{DPD} used through the MS mesostructure builder as input for DPD simulations for each salt concentration.[††] The experimental value for CMC of DTAC at room temperature reported in

[††] *In the MS mesostructure builder, the dimension units used to build simulation cells were set to reduced ones (i.e., DPD units). In order to generate the number of water and DTAC mesomolecules just as in Table 3, we have adjusted the reduced-density value to exactly 3, instead of the default 3.0833.*

Table 4. Aggregation Number N_{agg} of Micelles and their Apparition Frequency (Freq.), for Each Concentration c (in mol/kg) at the Final of DPD Simulations

$c_1=0.0050$		$c_2=0.0100$		$c_3=0.0151$		$c_4=0.0201$		$c_5=0.0252$	
N_{agg}	Freq.	N_{agg}	Freq.	N_{agg}	Freq.	N_{agg}	Freq.	N_{agg}	Freq.
1	34	1	46	1	42	1	49	1	46
2	2	2	6	2	9	2	9	2	12
		3	2	3	1	3	1	3	2
		12	1	4	2	4	1	4	1
				6	1	5	2	38	1
				8	1	6	2	71	1
				13	1	16	1		
				15	1	18	1		
						21	1		

$c_6=0.0302$		$c_7=0.0353$		$c_8=0.0404$		$c_9=0.0455$		$c_{10}=0.0507$	
N_{agg}	Freq.	N_{agg}	Freq.	N_{agg}	Freq.	N_{agg}	Freq.	N_{agg}	Freq.
1	44	1	35	1	38	1	36	1	39
2	5	2	5	2	6	2	7	2	7
3	1	3	1	3	1	3	1	3	3
26	1	28	1	8	1	4	1	4	2
34	1	36	1	15	1	9	1	5	1
54	1	46	1	16	1	12	1	6	1
56	1	52	1	23	1	24	1	18	1
		54	1	30	1	32	1	29	1
				36	1	34	1	46	1
				47	1	56	2	48	1
				74	1	60	1	49	1
								52	1
								54	1

literature is 0.0213 mol/kg.[55] Then, we performed DPD simulations from 0.005 to 0.0507 mol/kg (Table 3).[‡‡] The number of DPD simulation steps was 100,000, which was found to be sufficient to stabilize the micelle formation. The time step was 0.05 DPD units, and the mesomolecules positions were recorded each 100 steps. Figure 4 shows images of the DTAC distribution just at the step 100,000, where it has been omitted the water mesomolecules in the sake of a best visualization.

It can be seen that for the concentration $c_1=0.0050$ mol/kg, mesomolecules move around showing none tendency to associate with each other. At $c_2=0.0100$ mol/kg, some mesomolecules are grouped into small aggregates. At $c_3=0.0151$ mol/kg, the number of small aggregates raises. At $c_4=0.0201$ mol/kg, it is evident the growth of aggregate sizes, and at $c_5=0.0252$ mol/kg, the micelles appear in a new stable dispersed phase, as a direct consequence of the right chemistry, considered in evaluating the Flory–Huggins thermodynamics interaction parameters, contained into mesomolecules. Thereafter, the increase in concentration c increases the micelle number with similar sizes to that reached at c_5. Thus, the CMC is among 0.0201 and 0.0252 mol/kg. It is worthy to mention that the experimental value lies within this range.

In order to quantify the CMC more precisely, we have computed the aggregation number N_{agg} of the micelles formed at each concentration (Table 4) by defining the aggregate with a cutoff criterion: two surfactants belong to the same micelle if any of the beads in one mesomolecule is separated by less than r_{cutoff} from any bead of the another mesomolecule. For the DTAC-water system, $r_{cutoff}=\sqrt[3]{\rho V_b}=7.35$ Å (Eq. 14), where the V_b value is that reported in Table 1. Table 4 confirms the micelle evolution described earlier. Additionally, we observe that the value interval of aggregation number N_{agg} in general is split into two regions, one of small micelles owning an upper boundary at ~8 mesomolecules, and another one of high N_{agg} values starting from the medium size of ~10 mesomolecules. The apparition frequency for N_{agg} in the region of small micelles

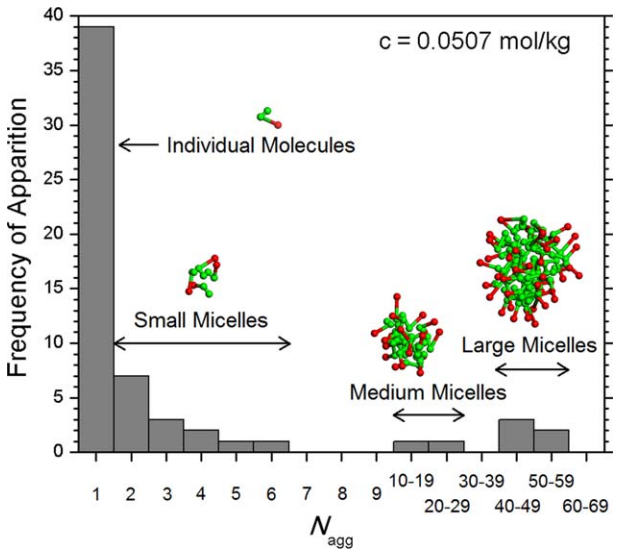

Figure 5. Histogram of the aggregation number N_{agg} for the concentration $c_{10}=0.0507$ mol/kg.

Insets: representative DTAC micelles with small, medium, and large sizes. [Color figure can be viewed in the online issue, which is available at wileyonlinelibrary.com.]

[‡‡] *Originally, concentrations at our work were screened from 0.005 to 0.050 M at steps of 0.005 M (i.e., in molarity units). The actual concentration range results from conversion to molality units.*

Table 5. Aggregate Radii R_{agg} ± their Standard Deviations for the 21 Micelles Found at the Concentration c_{10}=0.0507 mol/kg

N_{agg}	R_{agg} (Å)
2	5.39 ± 0.00
	6.57 ± 0.00
	7.02 ± 0.00
	7.77 ± 0.00
	7.92 ± 0.00
	9.46 ± 0.00
	9.88 ± 0.00
3	6.28 ± 0.54
	7.64 ± 1.07
	10.40 ± 0.90
4	7.93 ± 0.59
	10.76 ± 1.22
5	13.93 ± 1.56
6	10.29 ± 1.09
18	13.85 ± 1.18
29	17.13 ± 1.64
46	19.80 ± 2.15
48	22.02 ± 2.67
49	19.58 ± 1.74
52	20.38 ± 2.00
54	20.90 ± 1.71

decreases quickly with N_{agg} (Table 4 and Figure 5). For the greatest concentration, c_{10}=0.0507 mol/kg, the region of high aggregation number is composed of two subregions (Figure 5), the first one having two medium-size micelles with N_{agg} = 18 and 29 mesomolecules, and the second one having five large micelles with N_{agg} values among 46 and 54 mesomolecules. It is important to mention that the latter subregion is in excellent agreement with the experimental observed values for DTAC of N_{agg}^{exp}=47±5 molecules at concentrations near to the CMC and room temperature.[56] Similar simulation trends are shown by the concentrations c_6=0.0302 mol/kg, c_7=0.0353 mol/kg, c_8=0.0404 mol/kg, and c_9=0.0455 mol/kg, which possess large micelles with aggregation numbers distributed over intervals from 54 to 56, from 46 to 54, from 47 to 74, and from 56 to 60 mesomolecules, respectively. On the contrary, for low concentrations, that is, c_1, c_2, c_3, and c_4, mesomolecules are so separated to form stable large micelles. However, aggregate number increases with the concentration, so that at concentration c_5 the large micelles have been already found. At this concentration, the aggregation numbers fall out of the experimental values, may be due to the very few micelles existing in the region of high N_{agg}, as there are only two micelles in comparison with the seven micelles found for c_{10}.

Moreover, we have investigated the micellar size through the aggregate radius R_{agg}, defined here as the one half average of the maximum extension of a micelle measured from each mesomolecule.[§§] With the aim of having the best statistical description, we have calculated R_{agg} for each micelle at the concentration with the greatest population of micelles: c=c_{10} (Table 5). Aggregate radii for N_{agg} = 2, 3, and 4 mesomolecules increase as R_{agg} = 7.72, 8.11, and 9.35 Å, respectively, whereas for N_{agg} = 5 and 6 mesomolecules are R_{agg} = 13.93 and 10.29 Å, respectively. Thus, small micelles have aggregate radii lower than ~14 Å. Medium-size micelles, with N_{agg} = 18 and 29, have aggregate radii of R_{agg} = 13.85 and 17.13 Å, respectively. Large-size micelles, that is, those micelles with N_{agg} from 46 to 54 mesomolecules, have aggregate radii R_{agg} from 19.58 to 22.02 Å, in excellent concordance with literature experimental value of R_{agg}^{exp} = 20.1 Å.[57] Considering the standard deviation of R_{agg} for large micelles, the experimental aggregate radius R_{agg}^{exp} lies within the precision of the statistics of the computed radius as it is shown in Figure 6, in which it is also observed that thermal movement in general deviates somewhat the micelle morphology from the ideal spherical shape.

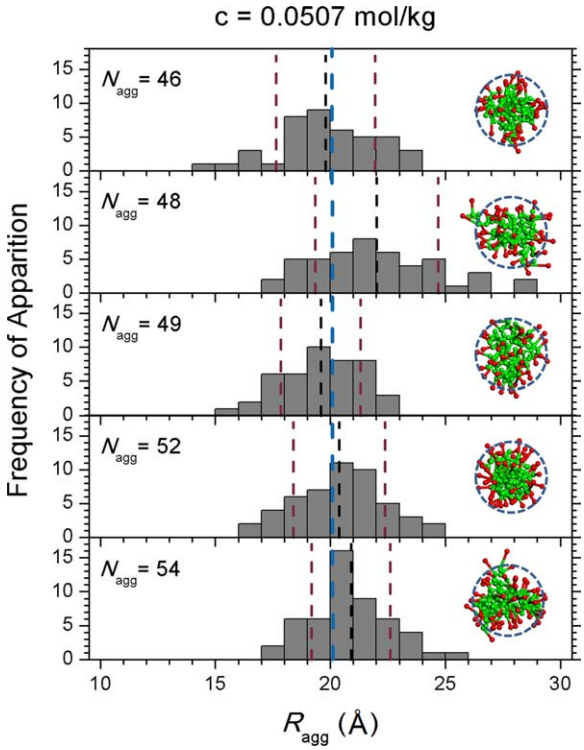

Figure 6. Histogram of the aggregate radius R_{agg} for the concentration c_{10} = 0.0507 mol/kg. Insets: DTAC micelles.

Dashed circumferences: guide to eye of ideal spherical micelles having the experimental radius R_{agg}^{exp}. Colors for dashed vertical lines: black, average of aggregate radii; dark red, limits of standard deviation; and blue, literature experimental value of R_{agg}. [Color figure can be viewed in the online issue, which is available at wileyonlinelibrary.com.]

Table 6. Fraction of Gathered DTAC Mesomolecules f_{gat} as Function of the Concentration c

c (mol/kg)	N_{agg}^{min}	N_{gat}^{DPD}	f_{gat} (%)
c_1=0.0050	0	0	0.000
c_2=0.0100	12	12	15.790
c_3=0.0151	8	36	31.858
c_4=0.0201	6	67	44.371
c_5=0.0252	4	113	59.788
c_6=0.0302	3	173	76.211
c_7=0.0353	3	219	82.955
c_8=0.0404	8	249	82.450
c_9=0.0455	4	287	84.412
c_{10}=0.0507	6	302	80.106

[§§] Formally, we define $R_{agg} \equiv \frac{1}{2}\langle \max_i \{||\mathbf{r}_j - \mathbf{r}_i||\}\rangle$ where $||\mathbf{r}_j - \mathbf{r}_i|| \equiv max_{\alpha,\beta}\left\{||\mathbf{r}_j^{\beta} - \mathbf{r}_i^{\alpha}||\right\}$ is, for a pair of DTAC mesomolecules i and j, the greatest of the distances over the beads α and β located at $\mathbf{r}_i^{\alpha}$ and $\mathbf{r}_j^{\beta}$, respectively, $\max_i\{d_{ij}\}$ is the maximum of the distances d_{ij} among mesomolecules i and j in a screening of mesomolecules i and a fixed mesomolecule j, and $\langle D_j\rangle$ is the average of the apparent diameters $\langle D_j\rangle$ of the micelle measured from mesomolecules j.

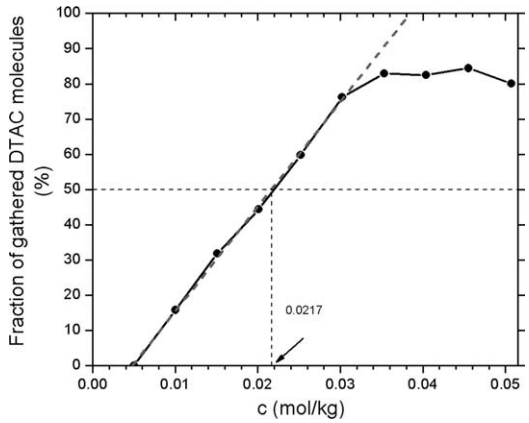

Figure 7. Fraction of DTAC mesomolecules gathered in micelles, f_{gat}, as function of DTAC concentration c in aqueous solution.

Gray dashed inclined line: linear regression fit at low concentrations (intercept: −0.14375, slope: 29.76021 kg/mol, and coefficient of determination: 0.99859).

By using the data of Table 4, we computed and plotted the fraction f_{gat} of DTAC mesomolecules gathered into micelles (Table 6 and Figure 7), that is, the ratio of the number of gathered DTAC mesomolecules, N_{gat}^{DPD}, to the total number of DTAC mesomolecules in the simulation cell, N_{DTAC}^{DPD} (Table 3). In obtaining the amount of gathered mesomolecules N_{gat}^{DPD}, we summed the number of mesomolecules over all micelles with aggregation number N_{agg} greater than, or equal to, the upper margin N_{agg}^{min} of the small micelles (Tables 4 and 6). From the fit of a straight line at low concentrations (Figure 7), it can be estimated a value for the CMC of 0.0217 mol/kg, since at this molality the adjusted gathered-molecules fraction f_{gat} reaches the value of 50%. When f_{gat} is just above 50%, a few micelles with large aggregation number begin to appear and contain most of the DTAC mesomolecules available in the system. It is expected that when concentration c increases, gathered-molecules fraction f_{gat} diminishes its slope to avoid crossing the 100% limit. Oscillations in f_{gat} after $c = 0.0353$ mol/kg are an effect of the saturation in the micelle number due to the simulation cell size.

Conclusions

Mesoscopic simulations performed to determine the CMC have been validated for DTAC in aqueous solution. DTAC and water atomic molecular models have been mapped onto mesomolecules composed of beads. We have then implemented a methodology to calculate interactions among beads based on quantum chemistry, in the framework of the DFT, in combination with statistical thermodynamics for liquids. The bead interactions so determined are taken into account in the mesoscopic simulations at DPD approximation, which provided a CMC among molalities 0.0201 and 0.0252 mol/kg. A better precise CMC estimation, through the fraction of gathered mesomolecules as a function of concentration, yields a value of 0.0217 mol/kg, in agreement with the measured value of 0.0213 mol/kg from literature. In the DTAC gathering process, it was observed the appearing of small micelles starting from 0.0100 mol/kg, and then both the amount of micelles and their sizes increase with concentration. When concentration reaches the value of 0.0252 mol/kg, some micelles achieve high aggregation numbers greater than around 40 mesomolecules. These large micelles are clearly distinguished from the small micelles possessing aggregation numbers less than 10 mesomolecules, which reveals concentration have been gone beyond the CMC. An analysis over the conformation of micelles produced at the major simulated concentration, which provides the best statistical description in this article, reveals that both aggregation number and aggregate radius for large micelles are also in agreement with the literature values of 47 ± 5 molecules and 20.1 Å, respectively, as the computed corresponding values lie in the range from 46 to 54 mesomolecules and from 19.58 to 22.02 Å. In this manner, by accomplishing the stringent criterion of matching simultaneously to experimental values the calculated CMC as well as the aggregation number and the size of the DTAC micelles in water, we have successfully showed that the original definition of the Flory–Huggins thermodynamic interaction parameters is an alternative, through quantum and statistical thermodynamics computed infinite-dilution activity coefficients, to the widely used methodologies in calculating DPD repulsive interactions based mainly on gas phase Monte Carlo and phase separation-oriented cohesive energy density.

Acknowledgments

Authors acknowledge to SENER-CONACYT-HIDROCARBUROS under grant number 146735 (Y.00123).

Literature Cited

1. Alvarado V, Manrique E. Enhanced oil recovery: an update review. *Energies*. 2010;3(9):1529–1575.
2. RezaeiDoust A, Puntervold T, Strand S, Austad T. Smart water as wettability modifier in carbonate and sandstone: a discussion of similarities/differences in the chemical mechanisms, *Energy Fuels*. 2009; 23:4479–4485.
3. Thomas MM, Clouse JA, Longo JM. Adsorption of organic-compounds on carbonate minerals. 1. Model compounds and their influence on mineral wettability. *Chem Geol*. 1993;109(1–4):201–213.
4. Rezaei Gomari KA, Denoyel R, Hamouda AA. Wettability of calcite and mica modified by different long-chain fatty acids (C18 acids). *J Colloid Interface Sci*. 2006;297(2):470–479.
5. Salehi M, Johnson SJ, Liang JT. Enhanced wettability alteration by surfactants with multiple hydrophilic moieties. *J Surfactants Deterg*. 2010;13(3):243–246.
6. Standnes DC, Austad T. Wettability alteration in chalk 2. Mechanism for wettability alteration from oil-wet to water-wet using surfactants. *J Petrol Sci Eng*. 2000;28(3):123–143.
7. Standnes DC, Austad T. Wettability alteration in carbonates: interaction between cationic surfactant and carboxylates as a key factor in wettability alteration from oil-wet to water-wet conditions. *Colloids Surf A*. 2003;216(1–3):243–259.
8. Strand S, Standnes DC, Austad T. Spontaneous imbibition of aqueous surfactant solutions into neutral to oil-wet carbonate cores: effects of brine salinity and composition. *Energy Fuels*. 2003;17(5): 1133–1144.
9. Standnes DC, Austad T. Wettability alteration in carbonates. Low cost ammonium surfactants based on bio derivatives from the coconut palm as active chemicals to change the wettability from oil-wet to water-wet conditions. *Colloids Surf A*. 2003;218(1–3):161–173.
10. Standnes DC, Austad T. Spontaneous imbibition of water into oil-wet carbonates. *J Petrol Sci Eng*. 2003;39(3–4):363–376.
11. Standnes DC, Austad T. Nontoxic low-cost amines as wettability alteration chemicals in carbonates. *J Petrol Sci Eng*. 2003; 39(3-4): 431–446.
12. Høgnesen E, Standnes DC, Austad T. Scaling spontaneous imbibition of aqueous surfactant solution into preferential oil-wet carbonates. *Energy Fuels*. 2004;18(6):1665–1675.

13. Standnes DC, Nogaret LAD, Chen HL, Austad T. An evaluation of spontaneous imbibition of water into oil wet carbonate reservoir cores using a nonionic and a cationic surfactant. *Energy Fuels*. 2002;16(6):1557–1564.
14. Jarrahian K, Seiedi O, Sheykhan M, Vafaie Sefti M, Ayatollahi S. Wettability alteration of carbonate rocks by surfactants: a mechanistic study. *Colloids Surf A*. 2012;410:1–10.
15. Fermeglia M, Pricl S. Multiscale molecular modeling in nanostructured material design and process system engineering. *Comput Chem Eng*. 2009;33(10):1701–1710.
16. Soto-Figueroa C, Rodríguez-Hidalgo MDR, Martínez-Magadán JM, Vicente L. Dissipative particle dynamics study of order–order phase transition of BCC, HPC, OBDD, and LAM structures of the poly (styrene)-poly (isoprene) diblock copolymer. *Macromolecules*. 2008; 41(9):3297–3304.
17. Rodríguez-Hidalgo MR, Soto-Figueroa C, Martínez-Magadán JM, Vicente L. Mesoscopic study of cylindrical phases of poly(styrene)-poly(isoprene) copolymer: order–order phase transitions by temperature control. *Polymer*. 2009;50(19):4596–4601.
18. Groot RD, Warren PB. Dissipative particle dynamics: bridging the gap between atomistic and mesoscopic simulation. *J Chem Phys*. 1997;107(11):4423–4435.
19. Li Y, Guo Y, Bao M, Gao X. Investigation of interfacial and structural properties of CTAB at the oil/water interface using dissipative particle dynamics simulations. *J Colloid Interface Sci*. 2011;361(2):573–580.
20. Chen Z, Cheng X, Cui H, Cheng P, Wang H. Dissipative particle dynamics simulation of the phase behavior and microstructure of CTAB/octane/1-butanol/water microemulsion. *Colloids Surf A*. 2007; 301(1–3):437–443.
21. Wei L, Ming Z, Jinli Z, Yongcai H. Self-assembly of cetyl trimethylammonium bromide in ethanol-water mixtures. *Front Chem China*. 2006;4:438–442.
22. Yuan SL, Cai ZT, Xu GY, Jiang YS. Mesoscopic simulation study on the interaction between polymer and C_{12}NBr or C_9phNBr in aqueous solution. *Colloid Polym Sci*. 2003;281(11):1069–1075.
23. Contreras-Pérez G. Modelación atómica y simulación mesoscópica de soluciones acuosas de surfactantes en la recuperación mejorada de hidrocarburos. Bachelor's Degree Thesis. Facultad de Estudios Superiores Cuautitlán, Universidad Nacional Autónoma de México, Estado de México, México, 2008.
24. Soto Escalante I. Determinación de las propiedades electrónicas y simulaciones molecular y mesoscópica de las interacciones surfactantes, n-decano, n-hexadecano, agua-dolomita. Bachelor's Degree Thesis. Facultad de Estudios Superiores Cuautitlán: Universidad Nacional Autónoma de México, Estado de México, México, 2010. Available at http://132.248.9.195/ptb2010/mayo/0657572/Index.html. Last accessed May 2, 2013.
25. Hoogerbrugge PJ, Koelman JMVA. Simulating microscopic hydrodynamic phenomena with dissipative particle dynamics. *Europhys Lett*. 1992;19(3):155–160.
26. Koelman JMVA, Hooggerbruge PJ. Dynamic simulations of hard-sphere suspensions under steady shear. *Europhys Lett*. 1993;21(3):363–368.
27. Kong Y, Manke CW, Madden WG, Schlijper AG. Simulation of a confined polymer in solution using the dissipative particle dynamics method. *Int J Thermophys*. 1994;15(6):1093–1101.
28. Schlijper AG, Hoogerbrugge PJ, Manke CW. Computer-simulation of dilute polymer-solutions with the dissipative particle dynamics method. *J Rheol*. 1995;39(3):567–579.
29. Maddalena V, Berend S. Simulating the self-assembly of model membranes. *PhysChemComm*. 1999;2(10):45–49.
30. Groot RD, Rabone KL. Mesoscopic simulation of cell membrane damage, morphology change and rupture by nonionic surfactants. *Biophys J*. 2001;81(2):725–736.
31. Espanol P, Warren P. Statistical-mechanics of dissipative particle dynamics. *Europhys Lett*. 1995;30(4):191–196.
32. Flory PJ. Principles of Polymer Chemistry. Ithaca, NY: Cornell University Press, 1953.
33. Case F, Honeycutt JD. Will my polymers mix? *Trends Polym Sci*. 1994;2(8):259–266.
34. Ryjkina E, Kuhn H, Rehage H, Müller F, Peggau J. Molecular dynamic computer simulations of phase behavior of non-ionic surfactants. *Angew Chem Int Ed*. 2002;41(6):983–986.
35. Hildebrand JH, Scott RL. The Solubility of Non-Electrolytes. New York: Reinhold, 1949.
36. Maiti A, McGrother S. Bead–bead interaction parameters in dissipative particle dynamics: relation to bead-size, solubility parameter, and surface tension. *J Chem Phys*. 2004;120(3):1594–1601.
37. Scocchi G, Posocco P, Fermeglia M, Pricl S. Polymer-clay nanocomposites: a multiscale molecular modeling approach. *J Phys Chem B*. 2007;111(9):2143–2151.
38. Lewars EG. Computational chemistry: Introduction to the theory and applications of molecular and quantum mechanics. Heidelberg, Germany: Springer, 2011.
39. Jensen JH. Molecular Modeling Basics. Boca Raton, FL: Taylor and Francis, CRC Press, 2010.
40. Jensen F. Introduction to Computational Chemistry. West Sussex, England: Wiley, 2007.
41. Klamt A, Eckert F. COSMO-RS: a novel and efficient method for the a priori prediction of thermophysical data of liquids. *Fluid Phase Equilib*. 2000;172(1):43–72.
42. Bondi A. van der Waals volumes and radii. *J Phys Chem*. 1964; 68(3):441–451.
43. IUPAC. Compendium of Chemical Terminology, 2nd ed. (the "Gold Book"). Compiled by McNaught AD, Wilkinson A. Oxford: Blackwell Scientific Publications, 1997.
44. Shulgin I, Ruckenstein E. Prediction of gas solubility in binary polymer + solvent mixtures. *Polymer*. 2003;44(3):901–907.
45. Zarkarian JA, Anderson FE, Boyd JA, Prausnitz JM. UNIFAC parameters from gas-liquid chromatographic data. *Ind Eng Chem Process Des Dev*. 1979;18(4):657–661.
46. Eckert F, Klamt A. Fast solvent screening via quantum chemistry: COSMO-RS approach. *AlChE J*. 2002;48(2):369–385.
47. TURBOMOLE V6.3 2011, a development of University of Karlsruhe and Forschungszentrum Karlsruhe GmbH, 1989–2007, TURBOMOLE GmbH, since 2007; available at http://www.turbomole.com. Last accessed May 2, 2013.
48. Klamt A, Schüürmann G. COSMO: a new approach to dielectric screening in solvents with explicit expressions for the screening energy and its gradient. *J Chem Soc Perkin Trans*. 1993;2(5):799–805.
49. Eckert F, Klamt A. COSMOtherm, Version C2.1, Release 01.11. Leverkusen, Germany: COSMOlogic GmbH and Co. KG, 2010.
50. Eckert F. COSMOtherm users manual, Version C2.1, Release 01.11. Leverkusen, Germany: COSMOlogic GmbH and Co. KG, 1999–2010.
51. Eichkorn K, Weigend F, Treutler O, Ahlrichs R. Auxiliary basis sets for main row atoms and transition metals and their use to approximate Coulomb potentials. *Theor Chem Acc*. 1997;97(1–4): 119–124.
52. Ahlrichs R, Bär M, Häser M, Horn H, Kölmel C. Electronic structure calculations on workstation computers: the program system turbomole. *Chem Phys Lett*. 1989;162(3):165–169.
53. Diedenhofen M, Klamt A. COSMO-RS as a tool for property prediction of IL mixtures—a review. *Fluid Phase Equilib*. 2010;294(1–2): 31–38.
54. Weast RC (ed). CRC Handbook of Chemistry and Physics. Boca Raton, FL: CRC Press, 1979.
55. Mehta SK, Bhasin KK, Chauhan R, Dham S. Effect of temperature on critical micelle concentration and thermodynamic behavior of dodecyldimethylethylammonium bromide and dodecyltrimethylammonium chloride in aqueous media. *Colloids Surf A*. 2005;255(1–3): 153–157.
56. Roelants E, De Schryver FC. Parameters affecting aqueous micelles of CTAC, TTAC, and DTAC probed by fluorescence quenching. *Langmuir*. 1987;3(2):209–214.
57. Bales BL, Zana R. Characterization of micelles of quaternary ammonium surfactants as reaction media I: dodeclytrimethilammonium bromide and chloride. *J Phys Chem B*. 2002;106(8):1926–1939.

Manuscript received Oct. 31, 2012, and revision received May 2, 2013.